ACS OMEGA

http://pubs.acs.org/journal/acsodf

Article

Three Dimensional Quercetin-Functionalized Patterned Scaffold: Development, Characterization, and *In Vitro* Assessment for Neural Tissue Engineering

Priya Vashisth, Neelakshi Kar, Deepak Gupta, and Jayesh R. Bellare*

Cite This: *ACS Omega* 2020, 5, 22325−22334

Read Online

ACCESS | Metrics & More | Article Recommendations

ABSTRACT: Regeneration of injured neuronal areas is a big challenge owing to the complex structure and function of the nervous system along with the limited regeneration capacity of neural cells. Recent reports show that patterned and functionalized scaffolds could control neural cell directional growth. In this study, aligned nanofibers (ANFs) were fabricated using a versatile and cost-effective approach, electrospinning, and further processed to make a patterned hybrid scaffold (HANF). The patterned scaffold had circular rings of ANFs reinforced in a biocompatible gellan−gelatin hydrogel matrix to provide adequate mechanical strength and contact guidance for adhesion and growth of neural cells *in vitro*. Quercetin was loaded into the nanofibrous scaffold to provide a functional agent that supported regeneration of neural cells. The reinforced ANFs enhanced the mechanical strength of the scaffold and provided a cylindrical nerve conduit structure to support neuronal cell growth. The influence of scaffold topology on cell behavior was assessed in *in vitro* cell culture conditions that revealed that the functionalized patterned scaffolds favored directed neurite cell growth/extension with favored cell culture morphology and showed no cytotoxicity toward neural cells. The results ultimately indicated that the fabricated scaffold has potential for guiding nerve tissue growth and can be used as nerve regeneration scaffolds.

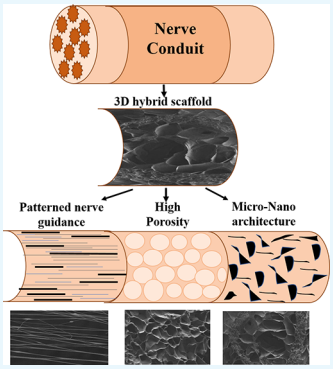

1. INTRODUCTION

Central and peripheral nerve injuries impact thousands of lives each year because of limited functional recovery of damaged neural tissue.[1−3] Damage to the neural tissue followed by trauma can create more defects and lead to substantial harm to nerve tissue which in turn require surgical intervention.[4,5]

At present, gold standard interventions for neural tissue repair involve autologous nerve grafting of less important nerves.[5,6] However, because of the issues such as availability and right size match are associated with the usage of autografts which limits its usage.[7] In such a scenario, the use of tissue-engineered scaffolds composed of mimetic biomaterials is recommended as an ideal futuristic choice.

A support structure as well as direct instillation of the required drugs/functional agent to injury sites can simply be achieved using biomaterials that possess analogous chemical and physical properties to natural extracellular matrix (ECM).[1,8,9] In addition, to support the regeneration of the damaged tissue, these biomaterials can provide suitable mechanical properties, high electrical conductivity,[10] unhindered mass transfer due to interconnected pores and high surface area,[11] biocompatibility, controlled bio-degradability, and an appropriate scaffold structure for cell overall growth in a three dimensional (3D) way.[12,13]

With regard to neural tissue engineering and regeneration, different biomaterials, such as hydrogels, peptide nanofibers and various aligned materials, have been proposed and studied.[13−16] However, unlike natural neural ECM, these scaffolds used to be structurally isotropic and therefore show less capability in directing the growth of cells in case of extensive neural tissue damage which requires directed neuronal reconnections. Therefore, to address this problem, here we introduce a biodegradable 3D-patterned scaffold to support guided neuronal growth. The scaffold comprises of aligned electrospun nanofibers made up of PVA−gelatin−gellan reinforced in a hydrogel matrix composed of gellan and gelatin in order to mimic the natural physical and chemical properties of neuronal ECM. Gellan and gelatin, both are well-known materials for tissue engineering purpose. The sustainability, biocompatibility, mild gelation conditions, structural similarity with native glycosaminoglycans, and tunable mechanical properties of gellan make it a potential choice for tissue regeneration application.[17−20] However, gellan alone lacks specific cell adhesion sites, which limits its usage as scaffolds.[21] Therefore, here we explored biofunction-

Received: June 7, 2020
Accepted: August 10, 2020
Published: August 25, 2020

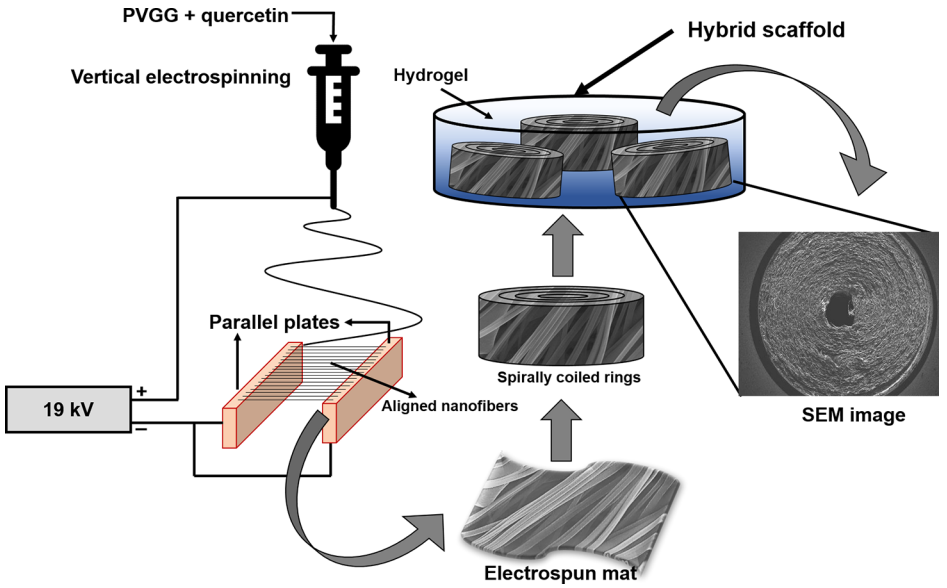

Figure 1. Schematic of the fabrication process for biomimetic circular conduit (HANF) for neural tissue regeneration.

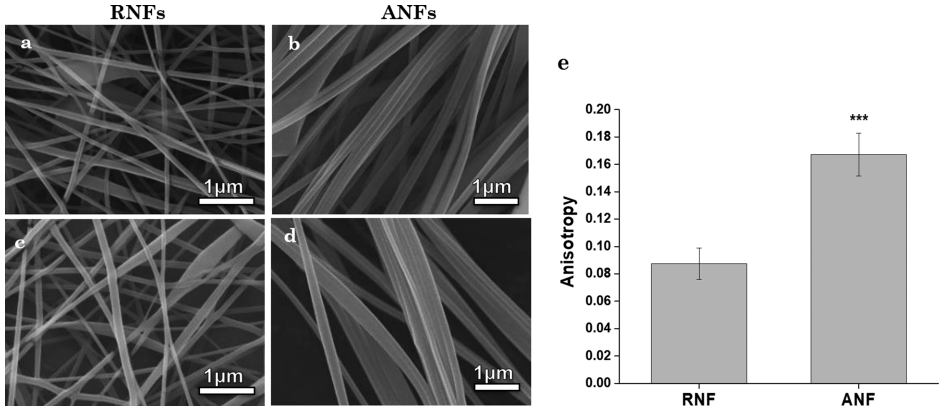

Figure 2. (a) SEM micrographs of PVGG RNFs, (b) PVGG ANFs, (c) quercetin-loaded PVGG-RNFs, (d) quercetin-loaded PVGG-ANFs, and (e) the anisotropy profile of RNFs and ANFs.

alization of gellan with gelatin. The gellan–gelatin hydrogels result in a self-standing hydrogel and was reported to provide a biomimetic environment as a natural ECM with relatively good cytocompatibility.[22,23] Moreover, the aligned nanofibers (ANFs), (considered as promising nanomaterials in facilitating nerve regeneration)[24−28] were reinforced in the gellan–gelatin hydrogel matrix in such a way that it can mimic the architecture of neural tissue and nanopattern-driven cues for guiding the growth of nerve cells.

More importantly, the fabricated nanofibers and the proposed scaffold designed in this study allow an easy yet effective way to encapsulate drugs within using an electrospinning approach. The efficacy of the fabricated HANF scaffold for drug delivery is demonstrated herein by incorporating "quercetin" as a model drug into the HANF. Quercetin possesses antioxidant and free radical scavenging properties, which are responsible for the prevention of oxidative stress-related diseases, such as neurodegenerative disorders.[29−31] Pandey et al. (2016) have reported positive effects of quercetin on Schwann cell proliferation and viability and their major role in nerve regeneration.[32] Many *in vitro* studies have revealed the role of quercetin in increased neuron survival and improved animal sensory and motor function recovery following peripheral nerve injury by increasing the intrinsic regeneration ability of neurons and preventing denervation at the distal stump.[33−35] Detailed experimental studies reported by Wang et al. (2011) in animals have shown that quercetin may improve the internal microenvironment of the fabricated neural bridge which in turn resulted in significant improvement in the maturity of regenerated nerves inside.[36]

In this study, we provided a means for safe and effective delivery of the quercetin drug to the defect site for improved viability and viability of SHY5Y neuronal cells. Further investigation of the role of quercetin on neuronal differentiation using more representative human neural cells and pluripotent stem cells needs to be conducted to provide a translational aspect to this work.

We further evaluated the feasibility of a single hybrid scaffold and its anisotropic structure to communicate the synergistic topographical and biochemical signals for proper neuronal tissue regeneration.[29,37,38] A recent study conducted by Wang el al (2019) discussed the role of biomimetic scaffolds for neural tissue engineering. Their results suggested that a 3D hierarchically aligned core–shell scaffold consisting of nanofibers and hydrogels can provide a 3D environment in order to

https://dx.doi.org/10.1021/acsomega.0c02678
ACS Omega 2020, 5, 22325−22334

induce neurite alignment and protect the nerve cell organization within it.[39]

Importantly, patterned and biofunctionalized scaffolds, that can control neural cell growth in a directive manner, hold much potential for neural tissue engineering.[40−43] This work demonstrates a unique 3D scaffold for neural tissue regeneration which unites two potential (hydrogel and ANFs) scaffolding systems into one to simultaneously provide mechanical support, directional channel, and biochemical cues.

2. RESULTS AND DISCUSSION

Two conductive strips (parallel plates) separated by a gap in between, facing electrostatic forces and acting in opposite directions, allow the fabrication of ANFs in the gap in a simplistic yet effective way.[44,45] A film or thick mat of these ANFs can also be collected in a timely manner through this technique for various applications. Figure 1 displays a schematic representation of the technique used to fabricate the biomimetic hybrid scaffold. To achieve a circular conduit of nanofibers (HANFs), spiral rings of ANFs with high mechanical strength were reinforced within a highly porous gellan−gelatin hydrogel matrix. Herein, compared to previous reports, we opted for this approach for the development of implantable biomimetic constructs with the ultimate goal to support and control neural directional growth, in order to attain functional neural regeneration.[28,41]

2.1. Morphology Analysis. FEGSEM micrographs of PVGG (quercetin free), quercetin-loaded PVGG random (PVGG-RNFs), and quercetin-loaded ANFs (PVGG-ANFs), depicting the morphology, distribution, and alignment of nanofibers, are shown in Figure 2. The average diameters of fibers were determined using ImageJ software and were recorded as 78 ± 52, 90 ± 51, 95 ± 24, and 108 ± 23 nm for PVGG-RNFs, quercetin-loaded PVGG-RNFs, PVGG-ANFs, and quercetin-loaded PVGG-ANF nanofibers respectively. Data obtained suggested that the diameter of nanofibers increased with the incorporation of quercetin.[46,47] Furthermore, FEGSEM micrographs of quercetin-loaded nanofibers depicted a smooth surface with the absence of any quercetin drug crystals on the outer surface of RNFs as well as on ANFs which confirms the acceptable incorporation of drug in the nanofibers (Figure 2c,d). As seen in the Figure 2e, the anisotropy value of the ANF scaffold is almost double that of the RNF scaffold. This confirms that fibers in ANF are aligned in the same direction. The RNF scaffold, as the name suggests, has randomly placed nanofibers, indicated by the SEM image and quantified by the anisotropy value.

An important aim of tissue engineering is to produce a scaffold which can replicate natural ECM formation by encouraging cell growth while maintain the desired cellular phenotype.[48,49] Following the same goal, in this study, we have reported a biomimetic hybrid scaffold (HANF scaffold) to provide a patterned platform comprising nano- to microscale features (Figure 3) and architectures in order to modulate the cell growth behavior through topological and biochemical mechanisms.

Figure 3 reveals the cross-sectional FEGSEM images of the HANF having circular rings of ANFs reinforced in a biocompatible gellan−gelatin hydrogel matrix. The cross-sectional view of ANF coils has been shown in Figure 3a,b. Figure 3c−f depicts the cross-sectioned view of HANF, that is, ANFs reinforced in the hydrogel matrix, gellan−gelatin hydrogel and reinforced ANFs, respectively. The hydrogel

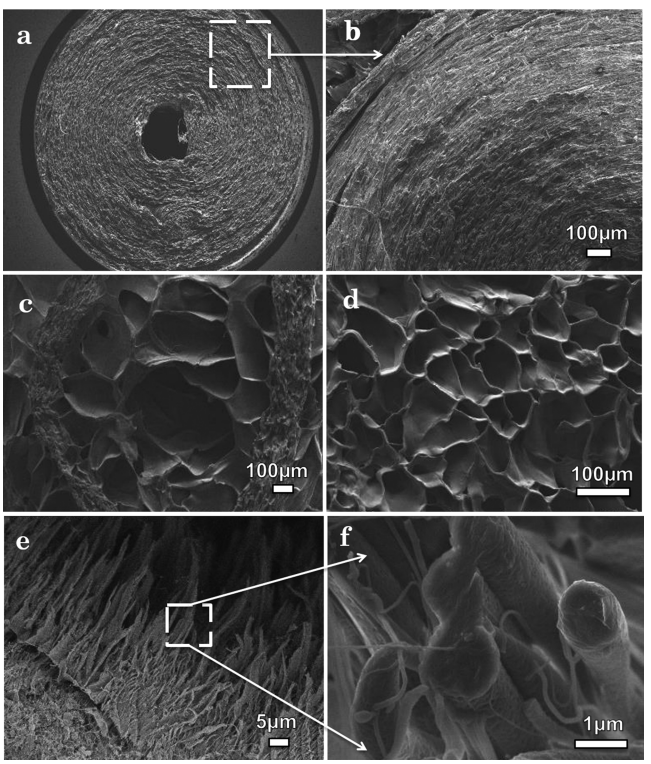

Figure 3. (a,b) SEM micrographs of cross-sectioned ANF circular conduit, (c) hybrid scaffold (HANF), (d) hydrogel, and (e,f) ANFs.

and nanofibers appear denser and bigger in diameter in contrast to the ones shown in Figure 2d because of the incorporation in the hydrogel matrix. Microscopic images were further used to determine the porosity of fabricated scaffolds. Hydrogel and HANF scaffolds show a combination of large and small pores, which promotes migration and infiltration of cells. The porosity values for hydrogel, ANF, and HANF were recorded to be 64.12 ± 6.48, 52.46 ± 11.02, and 31.92 ± 9.21%, respectively. The total porosity of HANF and ANF was less comparable to the hydrogel because of the tightly packed layers of ANFs; however, this was enough to promote cell migration through the scaffold to encourage cells regeneration. Furthermore, the circular conduit of nanofibers was designed in a way to provide similar topographical features and contact guidance as a natural neural ECM, which can provide a guided path for regrowth of neural cells *in vitro*.[24,25]

2.2. FTIR Analysis. The successful encapsulation of quercetin in PVGG electrospun nanofibers was comparatively analyzed from the IR spectrum of PVGG and quercetin-loaded PVGG ANFs (Figure 4A). The IR spectrum of native quercetin (Figure 4Ad) possessed typical absorption peaks for −OH groups (3406 cm^{-1}), C═O groups (1660 cm^{-1}), C−H groups (2800−2900 cm^{-1}), C−C groups (1591 cm^{-1}), C═C groups (1483 cm^{-1}), C−H stretching vibration (1425−1316, and 811 cm^{-1}), and C−O groups (1207, 1159−1002 cm^{-1}).[47,50] PVA (Figure 4Aa) and PVGG ANFs (Figure 4Ab) showed the IR bands at around 3320, 2923, and 1085−1720 cm^{-1} due to −OH and C−O groups, respectively.[51,52] However, some shifting in peaks toward the lower wavenumber was noticed in the case of PVGG nanofibers compared to PVA nanofibers, which suggests the noncovalent interactions between the polymers. The maximum of the peaks

https://dx.doi.org/10.1021/acsomega.0c02678
ACS Omega 2020, 5, 22325−22334

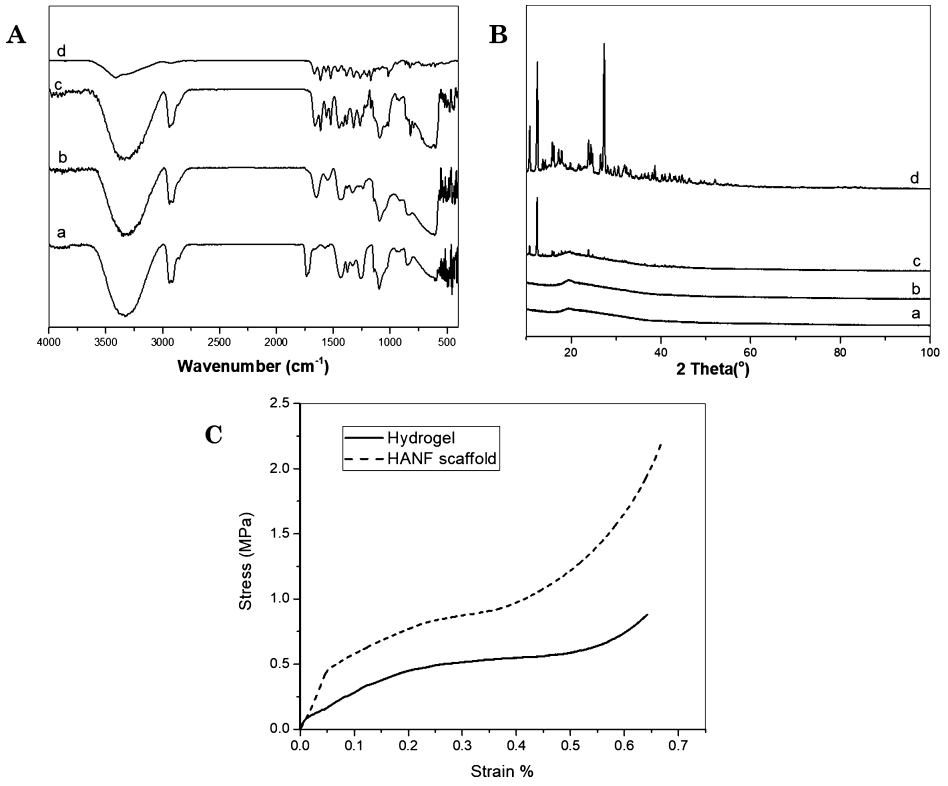

Figure 4. (A) FTIR spectrum of PVA (a), PVGG-ANFs (b), quercetin-encapsulated PVGG-ANFs (c), and quercetin (d). (B) XRD spectrum of PVA (a), PVGG-ANFs (b), quercetin-encapsulated PVGG-ANFs (c), and quercetin (d). (C) Stress v/s strain curve of gellan−gelatin hydrogel and the HANF.

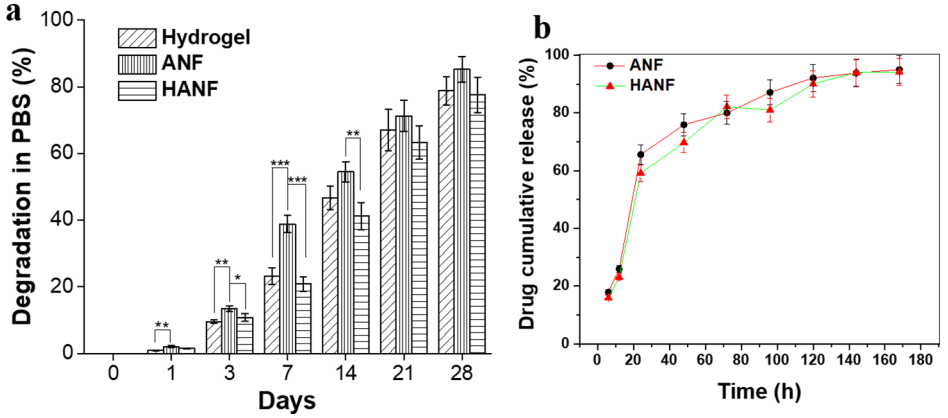

Figure 5. (a) Percent weight degradation of hydrogel, ANFs and HANF after day 1, 3, 7, 14, 21, and 28. Minimal weight loss was observed in the HANF scaffold after 28 days. (b) *In vitro* drug release profile of the quercetin drug from PVGG-ANF and HANF.

observed for quercetin-encapsulated nanofibers (Figure 4Ac) was found to be corresponded to the peaks present in the PVGG IR spectrum. Precisely, the presence of an absorption band at 3314, 2923, 1521, 1483, and 1178 cm^{-1}, attributed to the quercetin drugs, validated the occurrence of quercetin in the PVGG nanofibers.

The compatibility of quercetin with the polymeric matrix and its physical state in PVGG-ANFs were examined using XRD. Native quercetin was found crystalline with dominant peaks at 2θ = 11, 12.6, 16.1, 23.9, 27.3, and 38.6°, as shown in Figure 4Bd, while PVA (Figure 4Ba) and PVGG-ANFs (Figure 4Bb) without quercetin displayed broad amorphous peaks at 2θ = 19.3°. Distinct peaks were observed at 2θ = 10.6, 12.3, 16, 23.9, 27.3, 38, and 42.1° in the spectrum of quercetin-encapsulated PVGG nanofibers (Figure 4Bc) confirming the presence of semi-crystalline quercetin in PVGG-ANFs, which could be due to the large surface area of ANFs. The large surface area led to rapid solvent evaporation which permits limited time for recrystallization of drug and subsequently directs the formation of semi-crystalline or amorphous structures/matrix.[53,54]

2.3. Mechanical Properties of Scaffolds. Biomedical implants designed for tissue engineering and regeneration application should possess appropriate mechanical properties to provide adequate support to the affected area until the restoration of neo-ECM.[55,56] The hydrogel and nanofiber matrix alone do not comprise enough mechanical strength to support the proper neural cell attachment and proliferation

https://dx.doi.org/10.1021/acsomega.0c02678
ACS Omega 2020, 5, 22325−22334

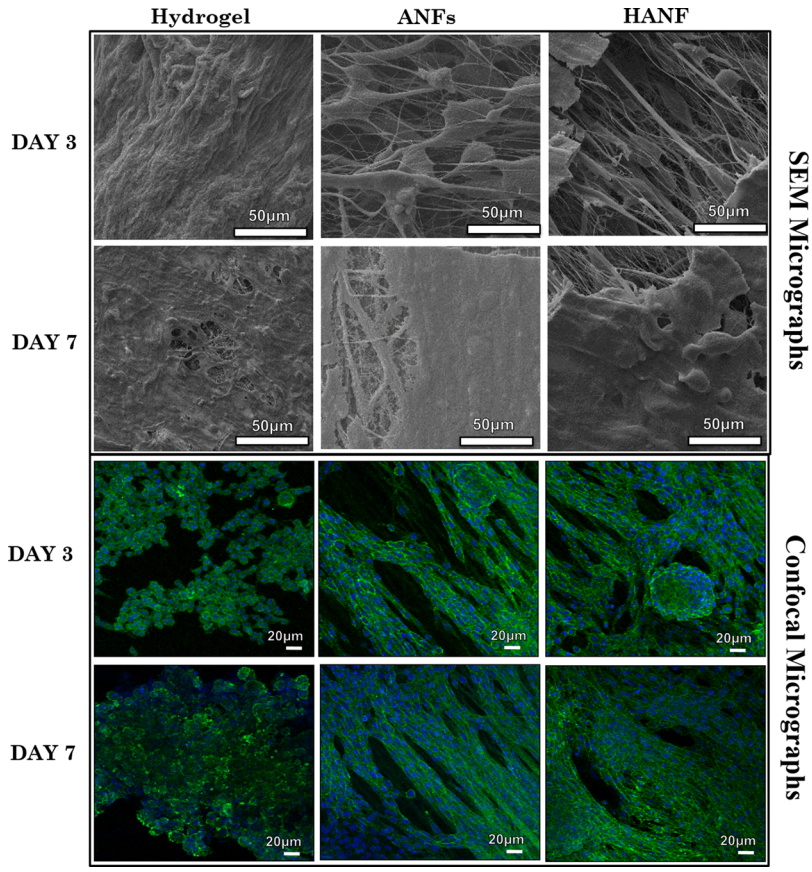

Figure 6. SEM and confocal micrographs (*z*-stacked) of SH-SY5Y cells grown on hydrogel, ANFs, and hybrid (HANF) scaffold after 3 and 7 days.

guidance.[7] Therefore, herein this study, we developed a hybrid scaffold (HANF) which consists of hydrogel reinforced with centrally coiled rings of ANFs. Figure 4C depicts the compressive strength of hydrogel- and nanofiber-enforced HANF scaffolds (circular nerve conduits). As expected, the gellan−gelatin hydrogel showed less moduli than ANFs and reinforced HANF scaffold. The maximum compressive strength recorded for the HANF scaffold was 2.21 MPa at a maximum strain of about 67% compared to gellan−gelatin hydrogel, for which the maximum compressive strength and compressive strain was recorded as 0.88 MPa at 64% maximum strain. Therefore, the compressive strength was found to be enhanced many folds in the case of HANF compared to nanofibers or hydrogel alone. This could be attributed to the reinforcement of ANFs in the hydrogel matrix, which could be further beneficial for the usage of these fabricated HANF in neural tissue engineering application.

2.4. Degradation Test. The *in vitro* degradation test and assessment of degradation profiles of scaffolds provide an indication of its degradation kinetics *in vivo*.[55,57] The weight loss profiles for all test samples (hydrogel, ANFs, and HANF scaffolds) after immersion in aqueous medium for set time periods are summarized in Figure 5a. As per our observation, the weight loss was found to be maximum for gellan−gelatin hydrogels, whereas minimum weight loss was observed in the case of quercetin-encapsulated HANF during the entire immersion period. The total weight loss noted at the end of the immersion period (28 days) was approximately 77% for patterned HANF compared to gellan−gelatin hydrogel and ANFs, for which it was approximately 80 and 86%, respectively. The results indicated that fabrication of HANF does not affect its stability.

The degradation rate was found similar in all the scaffolds. Although, hybrid scaffolds (HANF) were mechanically stronger than hydrogel. This could be because of the hierarchical difference in both the scaffolds. Materials used in both hydrogel and nanofibers were water soluble but cross-linked; however, the packing of the materials was entirely different in hybrid scaffolds. The dense packing of the aligned nanofibrous sheet, along with the fact that it was placed along its *z*-axis in the hydrogel, resulted in the higher compressive strength of HANF than hydrogel. Furthermore, our hypothesis indicates that the dense packing of ANFs in HANF did not affect the degradation rate because of the extremely high surface area of nanofibers, which when coupled with highly interconnected nano- and micro-porous structures led to unhindered water flow in and out of the construct, which in turn resulted in an unaltered degradation profile. The degradation rate further confirms that the scaffold is stable in PBS for 21 days without losing its integrity and thus can give support to cells for their growth and proliferation for sufficient time.

2.5. *In Vitro* Drug Release Profiles. The % EE of quercetin in PVGG-ANF was measured to be 74.17% using the pre-established protocols.[53,58] The *in vitro* drug release profiles of quercetin from PVGG-ANF and HANF have been depicted in Figure 5b. The release mechanism of the drug from the nanofibrous matrix in both types of scaffolds was chiefly attributed to the swelling of the polymeric matrix due to the fact that all the polymers used in the fabrication of nanofibers were hydrophilic. As soon as the PBS penetrated the polymeric

https://dx.doi.org/10.1021/acsomega.0c02678
ACS Omega 2020, 5, 22325−22334

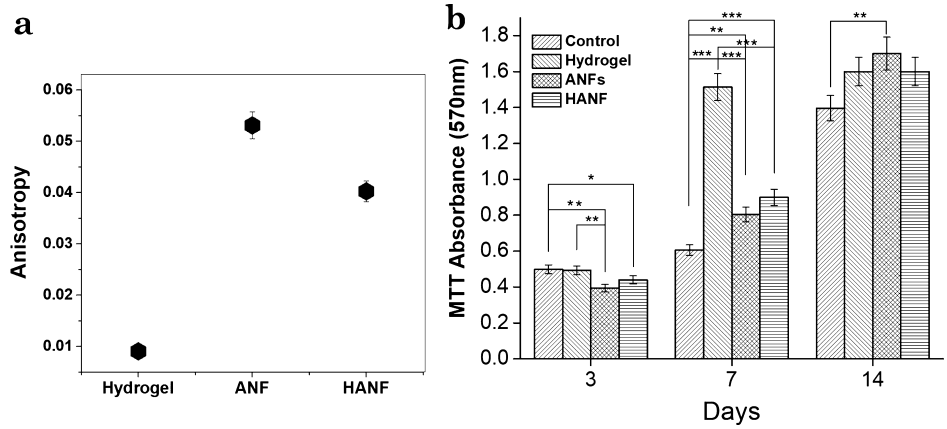

Figure 7. (a) Cell alignment study on the hydrogel, ANF, and HANF (b) viability assay absorbance results of SH-SY5Y cells on hydrogel, ANFs, and HANF after 3, 7, and 14 days.

matrix of scaffolds, it led to the diffusion of the quercetin drug into the external medium. The drug release mechanism was noticed to have two phases, first phase showed an initial burst release within 24 h of incubation where more than 60% of drug release was noticed from both the scaffolds followed by a sustained release (second phase), which was gradually extended up to 5 days. The initial burst release of the drug usually happens because of the diffusion of drug molecules accumulated on the surface of scaffolds,[59] whereas, the successive controlled release could be a result of diffusion of the drug molecules entrapped in the core region of the ANF matrix. In practice, both the phases are required to maintain the drug efficiency and optimum therapeutic level of the drug at the site of action.

2.6. Biocompatibility Studies. The *in vitro* cell culture results obtained herein supported our designed formulation and our hypothesis that the 3D biomimetic hybrid scaffolds fabricated with precise nano−micro-architecture and surface morphology can stimulate the cell behavior in a more appropriate way. This observation is also supported by previous studies and data.[60,61] The adhesion behavior of neural cells cultured on gellan−gelatin hydrogel, quercetin-loaded PVGG-ANFs, and HANF scaffold is depicted in Figure 6. The reported biomimetic HANF scaffolds allowed enhanced adhesion of neural cells along with their directed migration across the 3D scaffold. The vertical distribution of pores in the hydrogel matrix enabled the neural cells to infiltrate throughout the scaffold and therefore grow in different planes of the 3D-patterned scaffold. This is considered as a crucial cell growth activity for creating a favorable axonal environment and supporting neural tissue regeneration. Moreover, the cells cultured on HANFs were observed to align with the direction of nanofiber's alignment without influencing adhesion and proliferation.

Confocal images visualize the random distribution and round morphology of cells on hydrogel whereas patterned distribution and elongated morphology and ANFs and HANF. Through SEM analysis, we could only visualize and observe the cells present on the surface of the scaffold. Therefore, advanced confocal microscopic analysis was used to assess the cells deep in the planes of the 3D HANF scaffold. The cell-seeded test samples at different incubation points were observed for the analysis. The confocal imaging in a *z*-stack manner confirmed the improved cell adhesion and proliferation on HANF comparable to hydrogel after day 3 and 7 (Figure 6). In all scaffolds (hydrogels, ANFs, and HANF), cells were found to grow in different planes, and the *z*-stack confocal analysis further confirmed the abundant migration of cells in the deep layers of the hydrogel and HANF scaffold through the interconnective pores. In contrast, on ANFs, cells had a stretched morphology and their longitudinal axis was found to be aligned correspondingly with the direction of nanofibers compares to a round morphology on hydrogels at all-time points. The alignment of cells on different scaffolds can be interpreted from the data presented in Figure 7a. According to the previous reports, cells grown on pre-stressed directional surfaces elongate preferentially in the direction of the highest substrate stiffness as a result of the mechanotransduction effect faced by the cells on aligned surfaces.[62,63] However, the mechanism behind this phenomenon is not fully explained. Apart from the proper cell alignment, the migration and permeation of cells deep inside the nanofibrous scaffold was found to be limited because of the presence of smaller pores as compared to the hydrogel and HANF matrix. The SEM and confocal studies conclusively proved that the adhesion, migration, and proliferation of cells on biomimetic HANF led to the formation of distinct cell colonies that expanded both horizontally and vertically within the scaffold.

The biocompatibility results (MTT assay) collectively revealed that even with similar cell growth rates at all-time points (Figure 7b), there is a noticeable difference in cellular growth behavior including cell morphology, adhesion, and proliferation (Figure 6) on the HANF scaffold containing ANFs in contrast to hydrogel alone which has shown an elongated cell morphology and guided patterned cell growth compared to the round cell morphology and nonpatterned cell growth on hydrogel. The cells were grown in a more arranged fashion on ANFs as it should be in the case of neural tissue engineering. However, ANFs are two-dimensional matrixes which cannot properly mimic a similar environment as required for neural cell growth. In contrast, hydrogel represents the 3D matrix but lacks proper mechanical strength to support and initiate the early cell/tissue growth. Therefore, herein the 3D hybrid scaffold (HANF) has been discovered which can mimic the nerve circular conduit and behave like an in *vivo* neural tissue matrix. The developed 3D hybrid scaffold triggered the preferential orientation of neural cells as well as provided the improved mechanical strength because of the reinforcement of ANFs into it as compared to hydrogel alone.

https://dx.doi.org/10.1021/acsomega.0c02678
ACS Omega 2020, 5, 22325−22334

These data substantiate the feasibility of the patterned hybrid scaffold, reported herein, for effectively providing contact guidance and improved cell growth through topographical cues. However, these are the preliminary results and need further experimentation and substantial results to understand the exact mechanism behind it.

3. CONCLUSIONS

In this investigation, we presented a biomimetic 3D circular conduit scaffold comprising nano−microfeatures for neural tissue engineering. The scaffold has been designed by incorporating a high level of physiological similarity into intrinsic neural tissue ECM. The aligned PVGG nanofibers were reinforced in the hydrogel to mimic anatomical features of major nerves that have a central nerve core surrounded by swirls of myelin sheath. We used a well-established concept of nanopattern-driven cues for guiding the growth of nerve cells. Along with the biomimicry, reinforcement of nanofibers in hydrogel led to enhanced mechanical strength of the overall hybrid scaffold. Further, we examined the influence of the scaffold physical orientation on the neural cell growth. We conclude that the circular conduit (HANF) having an interconnected porous structure of the hydrogel matrix with nano-dimension-patterned fibers reinforced in between provides better mechanical strength compared to hydrogel or nanofibers alone, which in turn supports the enhanced cell adhesion, proliferation, migration, and neo-vessel formation throughout the scaffold. The designed and fabricated hybrid scaffold allowed the neural cells to attach, migrate, and proliferate in a more natural way compared to the matrix comprising aligned electrospun nanofibers alone. The results obtained collectively suggest that the scaffold reported herein with well-designed nano- and microarchitecture, comprising the benefits of two types of the 3D matrix and, can potentially be used for inducing specific biological stimuli for proper neural tissue regeneration.

4. EXPERIMENTAL SECTION

4.1. Materials. Gelatin type A was procured from Rama Industries, India. Polyvinyl alcohol (PVA: M_w—90,000), gellan gum (Gelzan; M_w—1000 kg/mol), fetal bovine serum (FBS), penicillin−streptomycin antibiotics, thiazolyl blue tetrazolium bromide (MTT), trypsin−EDTA, triton X-100, paraformaldehyde, dimethyl sulfoxide, glutaraldehyde, and other used chemical unless notified were procured from Sigma-Aldrich, India. Dulbecco's modified Eagle medium (DMEM) was purchased from Gibco, Invitrogen, USA.

4.2. Fabrication of the Nerve Guide Conduit/ Patterned HANF Scaffold. *4.2.1. Solution Preparation and Fabrication of Quercetin-Functionalized PVGG Nanofibers.* Aqueous solutions of PVA (10 wt %), gelatin (4 wt %), and gellan (2 wt %) were prepared separately. Gellan and gelatin solution were first mixed in an equal ratio and stirred for 6−8 h at 40 °C. PVA was then added in equal amounts in gellan/gelatin solution. The final ratio of polymers in the solution was accounted as 50:25:25 for PVA/gelatin/gellan (PVGG), respectively. The final solution was stirred overnight and kept for 1−2 h before electrospinning. For obtaining quercetin-functionalized PVGG nanofibers, 2 wt % of quercetin was dispersed in the final PVGG solution as described above. Electrospun PVGG nanofibers and quercetin-functionalized PVGG nanofibers were fabricated using a vertical electrospinning setup. Nanofibers were electrospun at a constant flow rate of 0.8 mL/h using, 19 kV of applied DC voltage and 15 cm working distance between a syringe tip and grounded collector. A flat aluminum collector was used to collect random nanofibers, whereas ANFs were fabricated on parallel plate electrodes with a 2 cm gap in between.

4.2.2. Preparation of Gellan−Gelatin Hydrogels. Gellan gum powder was dissolved in double distilled water at 90 °C under constant stirring to prepare clear aqueous solution of 2 wt % concentration. The properly dissolved transparent gellan gum solution was then allowed to cool down to 50 °C. At this maintained temperature, the pre-prepared gelatin solution (10 wt %) was added to gellan solution at equal ratios, which was additionally stirred for an hour. The final solution was poured into molds and kept in a vacuum desiccator overnight to remove any air space. The molded hydrogels were first frozen at −20 °C for approximately 2 h and then transferred to −80 °C for 24 h following by lyophilization to obtain the gellan−gelatin hydrogel scaffold.[55]

4.2.3. Fabrication of the Patterned Hybrid Scaffold (HANF). In order to prepare HANF, the flat sheets of nanofibers (approximately 0.04 mm thick) of ANFs were tightly coiled around a thin cylindrical wire to form a spiral-cylindrical column so that it can mimic the nerve conduit. The thickness of the nanofibrous sheets or coils can be controlled by varying the deposition time of nanofibers. The nanofibrous coils were then reinforced in gellan−gelatin hydrogel at about 50 °C (as below this temperature the gellan−gelatin solution starts to gel, which inhibits the proper integration of hydrogel with coaxial nanofibers). Figure 1 diagrammatically represents the HANF scaffold fabrication process. The molded HANF scaffolds were vacuum filtrated to avoid any air space between nanofibrous sheath and hydrogel matrix. The freezing and drying conditions were the same as described in the upper section for gellan−gelatin hydrogel.

4.3. Characterizations of the Nanofibrous Nerve Guide Conduit. *4.3.1. Fiber Morphology and Diameter Distribution Analysis.* The morphology of random and ANFs was observed using field-emission gun scanning electron microscopy (FEGSEM, FEI, Quanta 200 (D 7548)). For fiber diameter distribution analysis, different scaffolds were first fixed with 10% formalin at room temperature for an hour and then rinsed with PBS. Thereafter, the scaffolds were placed at −80 °C overnight. For imaging, the frozen scaffolds were cross sectioned in liquid nitrogen, sputter-coated with platinum for 120 s, and observed using FEGSEM at an accelerating voltage of 10 kV. The average fiber diameter and total porosity were measured using ImageJ software using three independent images (n = 3) of the scaffold. Alignment of fabricated nanofibers were quantified by finding the anisotropy value of the scaffolds from SEM images. This was done by Fibril Tool plugin of ImageJ software.[64]

4.3.2. FTIR Analysis. To ensure the presence of quercetin in the nanofibers and to study the possible interactions that may have happened between the drug and polymeric matrix, Fourier transform infrared spectroscopic analysis was carried out using a Nicolet Magna-IR FTIR 550 spectrophotometer (Nicolet Instrument Corporation, Madison, WI, USA). The IR absorption bands were recorded and presented in the scanning range of 4000−400 cm^{-1} with a resolution of 4 cm^{-1}.

4.3.3. XRD Analysis. The physical state of PVGG ANFs and quercetin-loaded ANFs was examined using a X-ray diffractometer (Rigaku Smartlab HRXRD). The XRD patterns were

https://dx.doi.org/10.1021/acsomega.0c02678
ACS Omega 2020, 5, 22325−22334

studied using Cu Kα radiation and reported over the 2θ range from 10 to 100° with a scanning rate of 2° min^{-1}.

4.3.4. Mechanical Properties. The comparative compressive properties of the hydrogel v/s HANF scaffold (sample size 10 × 10 mm) was measured in the completely dried state (lyophilized samples) using a Universal Testing Machine with a cross-head speed of 1 mm/min until 60% deformation of sample.

4.3.5. Degradation Test. *In vitro* degradation study of the test samples (hydrogel, ANFs, and HANF) was carried out by incubating the samples (n = 3) in PBS (pH 7.4) at 37 °C for pre-determined time periods. At different degradation points, the samples were taken out of PBS, washed with double distilled water, dried completely in a vacuum oven for 24 h, and weighed for analysis. Subsequently, the degradation index (D_i) for each sample was calculated using following equation:

$$D_i = (W_0 - W_t/W_0) \times 100$$

In this equation, W_0 represents the initial weight of the scaffold and W_t represents weight of the scaffold after a pre-determined time point.

4.4. *In Vitro* Drug Release Study. The *in vitro* drug release study of quercetin drug from PVGG-ANF and HANF (sample weight was approximately 20 mg) was performed by immersing them in phosphate buffer saline (PBS of pH 7.4; temperature 37 °C) for a period of 7 days. For assessment, 1 mL of samples' solution was withdrawn from dissolution medium at the predetermined incubation time. The withdrawn solution was used to take OD readings at 369 nm using UV−vis spectrophotometry. The cumulative release of quercetin from the ANFs and HANF was recorded as the function of incubation time.

4.5. Biocompatibility Studies. *4.5.1. Cell Culture.* SH-SY5Y cells (procured from NCCS Pune, India) were cultured in DMEM (Gibco) medium supplemented with 1% penicillin/streptomycin, 10% FBS at 37 °C maintaining 5% CO_2 in an incubator. The test samples (hydrogel, ANFs, and HANF) were cut into a proper size (10 mm × 10 mm) and sterilized with UV radiation for 1 h. Cells with a density of 2 × 10^4 cells per well were seeded on the different test samples along with DMEM culture medium and kept in a humidified atmosphere with 5% CO_2 at 37 °C.

4.5.2. Study of Cell Adhesion, Viability, and Migration. The adhesion behavior of neural cells on different test samples (hydrogel, ANFs, and HANF) was studied up to 7 days. For analysis, the cell-seeded scaffolds were first washed with PBS to remove any nonadherent cells. The attached cells were fixed with 2.5% glutaraldehyde solution, dehydrated in an ethanol solution through a graded series of alcohol (25, 50, 75, 90, and 100%) and were dried in a desiccator. The morphology of cells and adhesion behavior was then examined by using ESEM. To quantify a design encouraged cell orientation and migration across the scaffold, images of cells were taken using z-stack confocal microscopy. The alignments of the neural cells on different scaffolds were determined by observing the orientation of the cell nuclei within the SEM and confocal images as previously used by other groups.[27] Imaging was done on random fields covering different parts of the scaffold. For each sample type, three independent experiments for fluorescence imaging were done using 5−6 imaging fields for each repeat. This was done by Fibril Tool plugin of ImageJ software. The cell viability was measured after 3, 7, and 14 days of cell culture using a MTT assay.

4.6. Statistical Analysis. All statistical analysis was done in Origin 2018 data analysis software. One-way analysis of variance (ANOVA) was used for analyzing the data. The significant differences were calculated with post hoc Tukey's test. The significant differences were considered as *p < 0.05, **p < 0.01, and ***p < 0.001. The tested were performed for minimum two times with triplets of each sample. The graphs were plotted with mean ± standard deviation.

AUTHOR INFORMATION

Corresponding Author

Jayesh R. Bellare − *Wadhwani Research Centre for Bioengineering and Department of Chemical Engineering, Indian Institute of Technology Bombay, Mumbai, Maharashtra 400076, India;* orcid.org/0000-0002-6792-8327; Phone: +91 22 2576 7207; Email: jb@iitb.ac.in; Fax: +91 22 2572 6895

Authors

Priya Vashisth − *Wadhwani Research Centre for Bioengineering, Indian Institute of Technology Bombay, Mumbai, Maharashtra 400076, India;* orcid.org/0000-0003-4034-6543

Neelakshi Kar − *Department of Chemical Engineering, Indian Institute of Technology Bombay, Mumbai, Maharashtra 400076, India*

Deepak Gupta − *Department of Chemical Engineering, Indian Institute of Technology Bombay, Mumbai, Maharashtra 400076, India*

Complete contact information is available at: https://pubs.acs.org/10.1021/acsomega.0c02678

Notes

The authors declare no competing financial interest.

ACKNOWLEDGMENTS

The authors are grateful to Wadhwani Research Center for Bioengineering, Indian Institute of Technology Bombay for providing research support. We are also thankful to Central facilities and Centre for Research in Nanotechnology and Science (CRNTS), IIT Bombay for providing characterization facilities.

REFERENCES

(1) Xie, J.; MacEwan, M. R.; Schwartz, A. G.; Xia, Y. Electrospun Nanofibers for Neural Tissue Engineering. *Nanoscale* **2010**, *2*, 35−44.

(2) Sabelström, H.; Stenudd, M.; Réu, P.; Dias, D. O.; Elfineh, M.; Zdunek, S.; Damberg, P.; Göritz, C.; Frisén, J. Resident Neural Stem Cells Restrict Tissue Damage and Neuronal Loss after Spinal Cord Injury in Mice. *Science* **2013**, *342*, 637.

(3) Navarro, X.; Vivó, M.; Valero-Cabré, A. Neural Plasticity after Peripheral Nerve Injury and Regeneration. *Prog. Neurobiol.* **2007**, *82*, 163.

(4) Seidlits, S. K.; Lee, J. Y.; Schmidt, C. E. Nanostructured Scaffolds for Neural Applications. *Nanomedicine* **2008**, *3*, 183.

(5) Schmidt, C. E.; Leach, J. B. Neural Tissue Engineering: Strategies for Repair and Regeneration. *Annu. Rev. Biomed. Eng.* **2003**, *5*, 293.

(6) Lundborg, G. Nerve Regenration and Repair: A Review. *Acta Orthop. Scand.* **1987**, *58*, 145−169.

(7) Frost, H. K.; Andersson, T.; Johansson, S.; Englund-Johansson, U.; Ekström, P.; Dahlin, L. B.; Johansson, F. Electrospun Nerve Guide Conduits Have the Potential to Bridge Peripheral Nerve Injuries in Vivo. *Sci. Rep.* **2018**, *8*, 1−13.

(8) Dhandayuthapani, B.; Yoshida, Y.; Maekawa, T.; Kumar, D. S. Polymeric Scaffolds in Tissue Engineering Application: A Review. *Int. J. Polym. Sci.* **2011**, *2011*, 1−19.
(9) Patterson, J.; Martino, M. M.; Hubbell, J. A. Biomimetic Materials in Tissue Engineering. *Mater. Today* **2010**, *13*, 14.
(10) Chandrasekaran, S.; Yao, B.; Liu, T.; Xiao, W.; Song, Y.; Qian, F.; Zhu, C.; Duoss, E. B.; Spadaccini, C. M.; Li, Y.; Worsley, M. A. Direct Ink Writing of Organic and Carbon Aerogels. *Mater. Horiz.* **2018**, *5*, 1166−1175.
(11) Hanzawa, Y.; Kaneko, K.; Pekala, R. W.; Dresselhaus, M. S. Activated Carbon Aerogels. *Langmuir* **1996**, *12*, 6167.
(12) Guo, W.; Wang, S.; Yu, X.; Qiu, J.; Li, J.; Tang, W.; Li, Z.; Mou, X.; Liu, H.; Wang, Z. Construction of a 3D RGO-Collagen Hybrid Scaffold for Enhancement of the Neural Differentiation of Mesenchymal Stem Cells. *Nanoscale* **2016**, *8*, 1897−1904.
(13) Huang, C.-Y.; Hu, K.-H.; Wei, Z.-H. Comparison of Cell Behavior on Pva/Pva-Gelatin Electrospun Nanofibers with Random and Aligned Configuration. *Sci. Rep.* **2016**, *6*, 37960.
(14) Yang, F.; Murugan, R.; Wang, S.; Ramakrishna, S. Electrospinning of Nano/Micro Scale Poly(l-Lactic Acid) Aligned Fibers and Their Potential in Neural Tissue Engineering. *Biomaterials* **2005**, *26*, 2603.
(15) Abidian, M. R.; Martin, D. C. Multifunctional Nanobiomaterials for Neural Interfaces. *Adv. Funct. Mater.* **2009**, *19*, 573.
(16) Stabenfeldt, S. E.; García, A. J.; LaPlaca, M. C. Thermoreversible Laminin-Functionalized Hydrogel for Neural Tissue Engineering. *J. Biomed. Mater. Res., Part A* **2006**, *77A*, 718.
(17) Ng, J. Y.; Obuobi, S.; Chua, M. L.; Zhang, C.; Hong, S.; Kumar, Y.; Gokhale, R.; Ee, P. L. R. Biomimicry of Microbial Polysaccharide Hydrogels for Tissue Engineering and Regenerative Medicine − A Review. *Carbohydr. Polym.* **2020**, *241*, 116345.
(18) Geckil, H.; Xu, F.; Zhang, X.; Moon, S.; Demirci, U. Engineering Hydrogels as Extracellular Matrix Mimics. *Nanomedicine* **2010**, *5*, 469.
(19) Stevens, L. R.; Gilmore, K. J.; Wallace, G. G.; in het Panhuis, M. Tissue Engineering with Gellan Gum. *Biomater. Sci.* **2016**, *4*, 1276−1290.
(20) Oliveira, J. T.; Martins, L.; Picciochi, R.; Malafaya, P. B.; Sousa, R. A.; Neves, N. M.; Mano, J. F.; Reis, R. L. Gellan Gum: A New Biomaterial for Cartilage Tissue Engineering Applications. *J. Biomed. Mater. Res., Part A* **2010**, *93*, 852.
(21) da Silva, L. P.; Jha, A. K.; Correlo, V. M.; Marques, A. P.; Reis, R. L.; Healy, K. E. Gellan Gum Hydrogels with Enzyme-Sensitive Biodegradation and Endothelial Cell Biorecognition Sites. *Adv. Healthcare Mater.* **2018**, *7*, 1700686.
(22) Koivisto, J. T.; Gering, C.; Karvinen, J.; Maria Cherian, R.; Belay, B.; Hyttinen, J.; Aalto-Setälä, K.; Kellomäki, M.; Parraga, J. Mechanically Biomimetic Gelatin-Gellan Gum Hydrogels for 3D Culture of Beating Human Cardiomyocytes. *ACS Appl. Mater. Interfaces* **2019**, *11*, 20589−20602.
(23) Fedorovich, N. E.; Oudshoorn, M. H.; van Geemen, D.; Hennink, W. E.; Alblas, J.; Dhert, W. J. A. The Effect of Photopolymerization on Stem Cells Embedded in Hydrogels. *Biomaterials* **2009**, *30*, 344−353.
(24) Lee, J. Y.; Bashur, C. A.; Goldstein, A. S.; Schmidt, C. E. Polypyrrole-Coated Electrospun PLGA Nanofibers for Neural Tissue Applications. *Biomaterials* **2009**, *30*, 4325−4335.
(25) Berns, E. J.; Sur, S.; Pan, L.; Goldberger, J. E.; Suresh, S.; Zhang, S.; Kessler, J. A.; Stupp, S. I. Aligned Neurite Outgrowth and Directed Cell Migration in Self-Assembled Monodomain Gels. *Biomaterials* **2014**, *35*, 185−195.
(26) Gupta, D.; Venugopal, J.; Prabhakaran, M. P.; Dev, V. R. G.; Low, S.; Choon, A. T.; Ramakrishna, S. Aligned and Random Nanofibrous Substrate for the in Vitro Culture of Schwann Cells for Neural Tissue Engineering. *Acta Biomater* **2009**, *5*, 2560.
(27) Fee, T.; Surianarayanan, S.; Downs, C.; Zhou, Y.; Berry, J. Nanofiber Alignment Regulates NIH3T3 Cell Orientation and Cytoskeletal Gene Expression on Electrospun PCL+gelatin Nanofibers. *PLoS One* **2016**, *11*, No. e0154806.
(28) Gnavi, S.; Fornasari, B.; Tonda-Turo, C.; Laurano, R.; Zanetti, M.; Ciardelli, G.; Geuna, S. The Effect of Electrospun Gelatin Fibers Alignment on Schwann Cell and Axon Behavior and Organization in the Perspective of Artificial Nerve Design. *Int. J. Mol. Sci.* **2015**, *16*, 12925−12942.
(29) Cho, J.-Y.; Kim, I.-S.; Jang, Y.-H.; Kim, A.-R.; Lee, S.-R. Protective Effect of Quercetin, a Natural Flavonoid against Neuronal Damage after Transient Global Cerebral Ischemia. *Neurosci. Lett.* **2006**, *404*, 330.
(30) Wu, Y.; Sun, J.; George, J.; Ye, H.; Cui, Z.; Li, Z.; Liu, Q.; Zhang, Y.; Ge, D.; Liu, Y. Study of Neuroprotective Function of Ginkgo Biloba Extract (EGb761) Derived-Flavonoid Monomers Using a Three-Dimensional Stem Cell-Derived Neural Model. *Biotechnol. Prog.* **2016**, *32*, 735.
(31) Costa, L. G.; Garrick, J. M.; Roquè, P. J.; Pellacani, C. Mechanisms of Neuroprotection by Quercetin: Counteracting Oxidative Stress and More. *Oxid. Med. Cell. Longevity* **2016**, *2016*, 1.
(32) Pandey, A.; Patnaik, R.; Shukla, S.; Bhattacharya, P. A Possible Therapeutic Potential of Quercetin through Inhibition of μ-Calpain in Hypoxia Induced Neuronal Injury: A Molecular Dynamics Simulation Study. *Neural Regener. Res.* **2016**, *11*, 1247−1253.
(33) Jiang, W.; Luo, T.; Li, S.; Zhou, Y.; Shen, X.-Y.; He, F.; Xu, J.; Wang, H.-Q. Quercetin Protects against Okadaic Acid-Induced Injury via MAPK and PI3K/Akt/GSK3β Signaling Pathways in HT22 Hippocampal Neurons. *PLoS One* **2016**, *11*, No. e0152371.
(34) Ansari, M. A.; Abdul, H. M.; Joshi, G.; Opii, W. O.; Butterfield, D. A. Protective Effect of Quercetin in Primary Neurons against Aβ(1-42): Relevance to Alzheimer's Disease. *J. Nutr. Biochem.* **2009**, *20*, 269.
(35) Chen, M.-M.; Qin, J.; Chen, S.-J.; Yao, L.-M.; Zhang, L.-Y.; Yin, Z.-Q.; Liao, H. Quercetin Promotes Motor and Sensory Function Recovery Following Sciatic Nerve-Crush Injury in C57BL/6J Mice. *J. Nutr. Biochem.* **2017**, *46*, 57−67.
(36) Wang, W.; Huang, C.-Y.; Tsai, F.-J.; Tsai, C.-C.; Yao, C.-H.; Chen, Y.-S. Growth-Promoting Effects of Quercetin on Peripheral Nerves in Rats. *Int. J. Artif. Organs* **2011**, *34*, 1095−1105.
(37) Wang, Y.; Li, W.; Wang, M.; Lin, C.; Li, G.; Zhou, X.; Luo, J.; Jin, D. Quercetin Reduces Neural Tissue Damage and Promotes Astrocyte Activation after Spinal Cord Injury in Rats. *J. Cell. Biochem.* **2018**, *119*, 2298−2306.
(38) Taale, M.; Schütt, F.; Zheng, K.; Mishra, Y. K.; Boccaccini, A. R.; Adelung, R.; Selhuber-Unkel, C. Bioactive Carbon-Based Hybrid 3D Scaffolds for Osteoblast Growth. *ACS Appl. Mater. Interfaces* **2018**, *10*, 43874.
(39) Wang, L.; Wu, Y.; Hu, T.; Ma, P. X.; Guo, B. Aligned Conductive Core-Shell Biomimetic Scaffolds Based on Nanofiber Yarns/Hydrogel for Enhanced 3D Neurite Outgrowth Alignment and Elongation. *Acta Biomater.* **2019**, *96*, 175−187.
(40) Porzionato, A.; Barbon, S.; Stocco, E.; Dalzoppo, D.; Contran, M.; De Rose, E.; Parnigotto, P. P.; Macchi, V.; Grandi, C.; De Caro, R. Development of Oxidized Polyvinyl Alcohol-Based Nerve Conduits Coupled with the Ciliary Neurotrophic Factor. *Materials* **2019**, *12*, 1996.
(41) McMurtrey, R. J. Patterned and Functionalized Nanofiber Scaffolds in Three-Dimensional Hydrogel Constructs Enhance Neurite Outgrowth and Directional Control. *J. NeuSral. Eng.* **2014**, *11*, 066009−19.
(42) Chen, C.; Kong, X.; Lee, I.-S. Modification of Surface/Neuron Interfaces for Neural Cell-Type Specific Responses: A Review. *Biomed. Mater.* **2015**, *11*, 014108.
(43) Carvalho, C. R.; Wrobel, S.; Meyer, C.; Brandenberger, C.; Cengiz, I. F.; López-Cebral, R.; Silva-Correia, J.; Ronchi, G.; Reis, R. L.; Grothe, C.; et al. Gellan Gum-Based Luminal Fillers for Peripheral Nerve Regeneration: An: In Vivo Study in the Rat Sciatic Nerve Repair Model. *Biomater. Sci.* **2018**, *6*, 1059.
(44) Park, S. H.; Yang, D.-Y. Fabrication of Aligned Electrospun Nanofibers by Inclined Gap Method. *J. Appl. Polym. Sci.* **2011**, *120*, 1800.

https://dx.doi.org/10.1021/acsomega.0c02678
ACS Omega 2020, 5, 22325−22334

(45) Huang, C.-Y.; Hu, K.-H.; Wei, Z.-H. Comparison of Cell Behavior on Pva/Pva-Gelatin Electrospun Nanofibers with Random and Aligned Configuration. *Sci. Rep.* **2016**, *6*, 1−8.
(46) Vashisth, P.; Nikhil, K.; Pemmaraju, S. C.; Pruthi, P. A.; Mallick, V.; Singh, H.; Patel, A.; Mishra, N. C.; Singh, R. P.; Pruthi, V. Antibiofilm Activity of Quercetin-Encapsulated Cytocompatible Nanofibers against Candida Albicans. *J. Bioact. Compat. Polym.* **2013**, *28*, 652−665.
(47) Vashisth, P.; Singh, R. P.; Pruthi, V. A Controlled Release System for Quercetin from Biodegradable Poly(Lactide-Co-Glycolide)−Polycaprolactone Nanofibers and Its in Vitro Antitumor Activity. *J. Bioact. Compat. Polym.* **2016**, *31*, 260−272.
(48) Smith, I. O.; Ma, P. X. Biomimetic Scaffolds in Tissue Engineering. *Tissue Engineering: From Lab to Clinic*; Springer, 2011.
(49) Wang, X.; Ding, B.; Li, B. Biomimetic Electrospun Nanofibrous Structures for Tissue Engineering. *Mater. Today* **2013**, *16*, 229.
(50) Vashisth, P.; Nikhil, K.; Pemmaraju, S. C.; Pruthi, P. A.; Mallick, V.; Singh, H.; Patel, A.; Mishra, N. C.; Singh, R. P.; Pruthi, V. Antibiofilm Activity of Quercetin-Encapsulated Cytocompatible Nanofibers against Candida Albicans. *J. Bioact. Compat. Polym.* **2013**, *28*, 652−665.
(51) Vashisth, P.; Pruthi, P. A.; Singh, R. P.; Pruthi, V. Process Optimization for Fabrication of Gellan Based Electrospun Nanofibers. *Carbohydr. Polym.* **2014**, *109*, 16−21.
(52) Vashisth, P.; Pruthi, V. Synthesis and Characterization of Crosslinked Gellan/PVA Nanofibers for Tissue Engineering Application. *Mater. Sci. Eng., C* **2016**, *67*, 304−312.
(53) Vashisth, P.; Singh, R. P.; Pruthi, V. A Controlled Release System for Quercetin from Biodegradable Poly(Lactide-Co-Glycolide)−Polycaprolactone Nanofibers and Its in Vitro Antitumor Activity. *J. Bioact. Compat. Polym.* **2016**, *31*, 260−272.
(54) Vashisth, P.; Raghuwanshi, N.; Srivastava, A. K.; Singh, H.; Nagar, H.; Pruthi, V. Ofloxacin Loaded Gellan / PVA Nanofibers - Synthesis , Characterization and Evaluation of Their Gastroretentive/ Mucoadhesive Drug Delivery Potential. *Mater. Sci. Eng., C* **2017**, *71*, 611−619.
(55) Vashisth, P.; Bellare, J. R. Development of Hybrid Scaffold with Biomimetic 3D Architecture for Bone Regeneration. *Nanomedicine* **2018**, *14*, 1325−1336.
(56) Mata, A.; Kim, E. J.; Boehm, C. A.; Fleischman, A. J.; Muschler, G. F.; Roy, S. A Three-Dimensional Scaffold with Precise Micro-Architecture and Surface Micro-Textures. *Biomaterials* **2009**, *30*, 4610−4617.
(57) Mansur, H. S.; Costa, H. S.; Mansur, A. A. P.; Pereira, M. 3D-Macroporous Hybrid Scaffolds for Tissue Engineering: Network Design and Mathematical Modeling of the Degradation Kinetics. *Mater. Sci. Eng., C* **2012**, *32*, 404−415.
(58) Vashisth, P.; Raghuwanshi, N.; Srivastava, A. K.; Singh, H.; Nagar, H.; Pruthi, V. Ofloxacin Loaded Gellan/PVA Nanofibers - Synthesis, Characterization and Evaluation of Their Gastroretentive/ Mucoadhesive Drug Delivery Potential. *Mater. Sci. Eng., C* **2017**, *71*, 611−619.
(59) Chen, P.; Wu, Q.-S.; Ding, Y.-P.; Chu, M.; Huang, Z.-M.; Hu, W. A Controlled Release System of Titanocene Dichloride by Electrospun Fiber and Its Antitumor Activity in Vitro. *Eur. J. Pharm. Biopharm.* **2010**, *76*, 413.
(60) Li, Z.; Ramay, H. R.; Hauch, K. D.; Xiao, D.; Zhang, M. Chitosan-Alginate Hybrid Scaffolds for Bone Tissue Engineering. *Biomaterials* **2005**, *26*, 3919−3928.
(61) Liao, J.; Qu, Y.; Chu, B.; Zhang, X.; Qian, Z. Biodegradable CSMA/PECA/Graphene Porous Hybrid Scaffold for Cartilage Tissue Engineering. *Sci. Rep.* **2015**, *5*, 9879.
(62) Zhong, W.; Zhang, W.; Wang, S.; Qin, J. Regulation of Fibrochondrogenesis of Mesenchymal Stem Cells in an Integrated Microfluidic Platform Embedded with Biomimetic Nanofibrous Scaffolds. *PLoS One* **2013**, *8*, No. e61283.
(63) Nguyen, L. H.; Gao, M.; Lin, J.; Wu, W.; Wang, J.; Chew, S. Y. Three-Dimensional Aligned Nanofibers-Hydrogel Scaffold for Controlled Non-Viral Drug/Gene Delivery to Direct Axon Regeneration in Spinal Cord Injury Treatment. *Sci. Rep.* **2017**, *7*, 1−12.
(64) Boudaoud, A.; Burian, A.; Borowska-Wykręt, D.; Uyttewaal, M.; Wrzalik, R.; Kwiatkowska, D.; Hamant, O. FibrilTool, an ImageJ Plug-in to Quantify Fibrillar Structures in Raw Microscopy Images. *Nat. Protoc.* **2014**, *9*, 457.

https://dx.doi.org/10.1021/acsomega.0c02678
ACS Omega 2020, 5, 22325−22334